Hindawi
Journal of Sensors
Volume 2020, Article ID 4051474, 11 pages
https://doi.org/10.1155/2020/4051474

Research Article

Reduced Graphene Oxide/TEMPO-Nanocellulose Nanohybrid-Based Electrochemical Biosensor for the Determination of *Mycobacterium tuberculosis*

Mohd Hazani Mat Zaid,[1,2] Jaafar Abdullah,[1,3] Nor Azah Yusof,[1,3] Helmi Wasoh,[4] Yusran Sulaiman,[1,3] Mohd Fairulnizal Md Noh,[5] and Rahizan Issa[6]

[1]*Institute of Advanced Technology, Universiti Putra Malaysia, 43400 UPM Serdan, Selangor D.E., Malaysia*
[2]*Centre for Advanced Materials and Renewable Resources, Faculty of Science and Technology, Universiti Kebangsaan Malaysia, 43600 Bangi, Selangor, Malaysia*
[3]*Department of Chemistry, Faculty of Science, Universiti Putra Malaysia, 43400 UPM Serdang, Selangor Darul Ehsan, Malaysia*
[4]*Department of Bioprocess Technology, Faculty of Biotechnology and Biomolecules Sciences, Universiti Putra Malaysia, 43400 UPM Serdang, Selangor Darul Ehsan, Malaysia*
[5]*Cardiovascular Diabetes and Nutrition Research Centre, Institute for Medical Research, Jalan Pahang, 50588 Kuala Lumpur, Malaysia*
[6]*Bacteriology Unit, Infectious Disease Research Centre, Institute for Medical Research, Jalan Pahang, 50588 Kuala Lumpur, Malaysia*

Correspondence should be addressed to Jaafar Abdullah; jafar@upm.edu.my

Received 25 September 2019; Revised 22 November 2019; Accepted 14 December 2019; Published 21 January 2020

Academic Editor: Hai-Feng Ji

A novel peptide nuclide acid (PNA) electrochemical biosensor based on reduced graphene oxide (NH_2-rGO)/2,2,6,6-tetramethylpiperidin-1-yl)oxyl nanocrystalline cellulose (TEMPO-NCC) for the detection of *Mycobacterium tuberculosis* (*M. Tuberculosis*) is described. In this study, the nanohybrid films NH_2-rGO/TEMPO-NCC were immobilized onto screen-printed carbon electrode (SPE) via a simple drop-coating method. The electrochemical characterization of the designed electrode was investigated using cyclic voltammetry (CV) and impedance spectroscopy (EIS). Meanwhile, the sensitivity and selectivity of the designed biosensor against *M. tuberculosis* were measured by the differential pulse voltammetry (DPV). The response of the PNA probe-modified (NH2-rGO)/TEMPO-NCC demonstrated that the fabricated biosensor was able to distinguish between complementary, noncomplementary, and one-base mismatch DNA sequences using methylene blue (MB) as the electrochemical indicator. The developed electrochemical biosensor exhibited a linear calibration curve in the concentration range of 1×10^{-8} M to 1×10^{-13} M with the limit of detection of 3.14×10^{-14} M. The developed electrochemical biosensor has also been tested with a polymerase chain reaction (PCR) product of *M. tuberculosis* DNA which has shown successful results in distinguishing between negative and positive samples of M. tuberculosis.

1. Introduction

Tuberculosis (TB) bacteria, commonly attack human lung caused by *M. tuberculosis*, was first spotted by Robert Koch in 1882 [1]. In 2017, there were around 1.6 million TB deaths, including 300,000 people living with HIV [2]. This significantly urges countries with many HIV-associated TB patients to rapidly integrate and scale up their TB/HIV services to reduce the number of deaths. Therefore, early-stage TB screening for people diagnosed with HIV is important, and the delay between diagnosis and treatment must be drastically reduced [3]. There are many literatures related to diagnostic techniques for detecting *M. tuberculosis* have been reported. For instance, tuberculin skin test [4] and acid-fast staining [5] are the most commonly used techniques. Meanwhile, chest radiograph [6], polymerase chain

reaction (PCR) assay, Xpert MTB/RIF [7], and immunological tests [8] are the best options to shorten the diagnosis time to a few hours compared to conventional techniques which required several days. However, majority of the conventional diagnostic techniques have their limitations such as labour intensiveness, complex working protocol, and costly reagents [9].

The existence of limitations owing to a conventional method has urged the development of new alternative approaches towards real-time diagnosis for rapid, sensitive, simple, and convenient to use. Therefore, the exceptional potentiality of biosensors in tuberculosis diagnostics has stimulate an evolution and innovating advanced tools such as surface plasmon resonance (SPR) biosensors [10], piezoelectric biosensors [11], optical biosensor [12], and magnetoelastic biosensors [13]. Despite the reported biosensors which displayed a spectacular performance towards TB detection, its lack of sensitivity is the main considerable concern for its performance particularly to meet criteria setup by World Health Organization (WHO). Considering this fact, the DNA-based electrochemical sensor which is capable of meeting the criteria established by WHO had offered an attractive platform for affordable, user friendly, rapid, and robust development of point-of-care (POC) diagnostic [14]. The abreast electrochemical biosensor is not only free of complications in operation and sample handling but also provides highly sensitive and specific measurements for a wide-ranging biomolecules [15].

Compared to DNA, peptide nucleic acid (PNA) recognition layers have been proven more prevalence for sequence-specific DNA biosensors and provide a lot of application in numerous fields [16, 17]. As previously reported, PNA was able to leverage the sensitivity and specificity detection and shows greater discrimination against single-base mismatches. Likewise, PNA also shortens hybridization time at room temperatures and lessens dependence on ionic strength [18, 19].

To date, technology based on screen printing technology has successfully produced by commercially available screen-printed electrode (SPE) which offers the possibility for miniaturization, disposable, and lower cost product towards point-of-care (POC) device development [20]. Meanwhile, SPE based on carbon was popular in electrochemical biosensor development due to its intriguing properties such as chemically inert, low background currents, and wide potential window [21].

Typically, modification of the working electrode remains an important strategies for the fabrication of reproducible, stable, and selective biologically modified surfaces [22, 23]. The modified electrode with biorenewable polymer-based nanomaterials has been found to improve the sensitivity of the biosensor especially for the electrochemical DNA biosensor as shown in the previous studies [24, 25]. One of the materials is nanocrystalline cellulose (NCC) which is new nanomaterial with an inherent high surface area, is easily functionalized, biocompatible, and eco-friendly, and has feasible requirement to develop a sensitive biosensor [26, 27]. Besides, NCC has also been studied in a wide range of potential application with other composite materials that enable to be used in various applications such as a carrier for enzyme and protein [28, 29]. In spite of having its own unique properties, NCC are also impaired from poor electrical conductivity which is not practically desired in an electrochemical biosensor. To alleviate its nature property limitations, NCC can be grafted with various foreign monomers through chain reaction to turn NCC into a customizable material [30].

On the other hand, reduced graphene oxide (rGO) has gained a combination of excellent electrical conductivity and a large surface area shows the capability to promote electron transfer and further amplifies the electrochemical signal [31]. Reduced graphene oxide (rGO) or synonyms as functionalized graphene oxide [32] provides abundant structural defects and accessible functional groups which advantages as an immobilization matrix for biological element recognition. Hence, it is expected that rGO-based hybrid materials can further improve the performance of electrochemical biosensors [33].

In this work, we explore a novel electrochemical PNA biosensor based on screen-printed carbon electrode- (SPE-) modified TEMPO-nanocrystalline cellulose (TNCC) composite with amine-functionalized reduced graphene oxide (NH_2-rGO) for *M. tuberculosis* detection. The fabricated PNA electrochemical biosensor is capable of detecting the target DNA-related TB as low as subpico molar, as well as recognizing various DNA sequences including complementary, one-base mismatch, and noncomplementary. The result of the fabricated electrochemical-based PNA offered excellent analytical performances for the detection of high sensitivity, wide linearity range, and lower detection limit for the TB bacterial detection. Moreover, an attempt has been made to detect the presence of a complementary target in the PCR product of *M. tuberculosis*. To the best of our knowledge, integration nanohybrid material based on nanocrystalline cellulose with reduced graphene oxide has not been extensively studied for the development of an electrochemical biosensor for the detection of *M. Tuberculosis*.

2. Experimental

2.1. Apparatus. Cyclic voltammetry, differential pulse voltammograms (DPV), and electrochemical impendence spectroscopy (EIS) were performed using Autolab PGSTAT204 (Netherlands) controlled by the computer. Screen-printed carbon electrode (SPE) (diameter = 4 mm) was purchased from Rapid Genesis Sdn Bhd (Malaysia) which consists of the working electrode (carbon), reference electrode (AgCl), and an auxiliary electrode (carbon), respectively.

2.2. Chemical. Water dispersion graphene oxide (0.4 wt% concentration) was purchased from Graphenea (Spain). Nanocrystalline cellulose (NCC) was acquired from the University of Maine (USA). Ethylenediamine (EDA), potassium ferricyanide ($K_3[Fe(CN)_6]$), N-hydroxysuccinimide (NHS), N-ethyl-N-(3-(dimethylaminopropyl) carbodiimide (EDC), methylene blue (MB), and all other chemicals were purchased from Sigma-Aldrich (Malaysia). Peptide nucleic acid (PNA) was synthesized by Panagene Co. (Korea), while DNA was synthesis by First BASE Laboratories Sdn. Bhd (Malaysia). The PNA and oligonucleotide sequence used in

this work were based on the previous work by Issa et al. [34], with the following sequences: ssPNA probe, 5′-CTCGTC CAGCGCCGCTTCGG-3; target DNA, 5′-CCGAAGCGG CGCTGGACGAG-3; noncomplimentary, 5′-TTTGGTATT ATTGTTCATGT-3′; and one-base mismatch, 5′-CCGA AGCGGCGCTGGACGAT-3′. Meanwhile, five DNA clinical samples were collected from sputum specimens of TB-infected persons provided by the Institute for Medical Research (IMR), Malaysia.

2.3. Preparation of TEMPO-Nanocrystalline Cellulose (TNCC). TEMPO-nanocrystalline cellulose was prepared based on the method previously reported by Fukuzumi et al. [35]. Firstly, nanocrystalline cellulose powder (1.0 g) was dissolved in deionized water (100 mL) containing TEMPO (0.016 g, 0.1 mmol) and NaBr (0.1 g, 1.0 mmol). The resulting slurry solution was added with NaClO solution (3.1 g, 5.0 mmol), and the mixture was stirred for 15 min at room temperature to achieve a complete reaction. Then, 0.5 NaOH was slowly added dropwise until pH 10 was reached.

2.4. Preparation of NH_2-rGO/TNCC. The method to reduce graphene oxide was carried out according to the procedure described in our previous work [36]. The process was carried out using ethylenediamine as reducing agents to produce amine reduced graphene oxide (NH_2-rGO). Herein, 1 mL of ethylenediamine (EDA) was slowly added into 3 mg/mL of graphene oxide with vigorous stirring. The homogenous mixture was then added with N-ethyl-N-(3-(dimethylaminopropyl) carbodiimide (EDC) (60 mg) until the suspension was slowly dissolved. The resulting suspension was continuously stirred until its colors turn from brown to dark black. The obtained suspension was then washed using ethanol and centrifuged at 4000 rpm for 5 min to remove any excessive EDA and EDC. This process was repeated for 5 times before it is further dried in the oven at 60°C for 1 h to obtain fine NH_2-rGO slurry. Subsequently, the obtained product of NH_2-rGO (200 mg) was dispersed in 1% (*w*/*v*) of TNCC solution using an ultrasonic bath for 30 min. The prepared sample has been identified as NH_2-rGO/TNCC.

2.5. Preparation of SPE-Modified NH_2-rGO/TNCC. Prior to electrode modification, pretreatment of the SPE is necessary to activate the carbon electrode surface. SPE was pretreated by the cyclic voltammetry (CV) for ten cycles in the potential range of +0.1 V to +0.7 V and the scan rate of 50 mV/s in 0.1 M phosphate buffer solution (PBS). Then, 7 μL of the NH_2-rGO/TNCC mixture was drop cast onto the SPE surface and kept at room temperature for the drying process.

2.6. Immobilization of PNA Probe. The immobilization procedure of PNA was started by immersion of NH_2-rGO/TNCC/SPE into a solution containing EDC/NHS (6 mM/5 mM) at room temperature for 1 hour. Afterward, a drop of a PNA probe (3 μL) with concentration of 5 μM was added onto activated NH_2-rGO/TNCC/SPE and kept at 18°C for 1 hour. Subsequently, the modified SPE was rinsed with phosphate buffer solution (pH 7) to remove any unbound PNA probe. The resulting modified electrode was denoted as NH_2-rGO/TNCC/PNA/SPE.

2.7. Hybridization Process. About 2 μL of target DNA solution with the desired concentration was dropped onto the PNA immobilized electrode and incubated at 40°C for 30 min. Then, phosphate buffer solution (pH 7) was used to wash the unhybridized probe and to remove imperfectly matched hybrid. Subsequently, the hybridized electrode was immersed into methylene blue (MB) (45 μM) in phosphate buffer solution containing 20 mM NaCl (pH 7) for 5 min. After the accumulation, the electrode was rinsed again with phosphate buffer solution to remove any unbound MB molecules. Lastly, the electrode was transferred into 0.1 M phosphate buffer solution (pH 7.0) and ready for electrochemical analyses.

2.8. PCR Amplification. To examine reliability of the fabricated biosensor with real sample, PCR amplification targeting IS6110 for the detection of MTB was also performed. *Mycobacterium genomic* DNA was used as the template DNA using MTB forward (5′-CTC TGG ACA GAG AGT ATT TGG-3′) and MTB reverse (5′-TGC AAT GTT AAG TTT AGT AGC AG-3′), respectively. For sample preparation, sputum sample obtained from TB patients confirmed through smear microscopy for the presence of acid-fast bacilli and by culture for the growth of MTB was used. Then, it was confirmed positive *M. Tuberculosis* by running PCR mixture in 1% agarose gel for 45 min, and the samples were observed under ultraviolet light. The general procedure for fabrication of the electrochemical PNA biosensor can be summarized in Schematic 1.

3. Results and Discussion

3.1. Morphological Characterization. Morphological characterization of nanohybrid material (NH_2-rGO/TNCC) with higher magnification of FESEM image (10,000x) was carried out to see qualitative data of the prepared NH_2-rGO, TNCC, and NH_2-rGO/TNCC, respectively. In Figure 1(a), NH_2-rGO shows wrinkle, and corrugated morphology due to disruption and impairments of GO resulted from chemical reduction by ethylenediamine (EDA) [37, 38]. Furthermore, the FESEM images of TNCC shown in Figure 1(b) display a rod-like individualize nanoparticle image as a result of electrostatic repulsion between fibers and keep it separated [39]. Meanwhile, in Figure 1(c), the FESEM image of the reduced graphene oxide NH_2-rGO/TNCC revealed that wrapping sheet formation of NH_2-rGO attached to fiber structure of TNCC had prevented the nanohybrid from agglomeration.

3.2. FTIR Characterization. To observe the interaction between NH_2-rGO and TNCC, FTIR characterization was performed to confirm the interaction between NH_2-rGO and TNCC. Figure 2(a) illustrates the FTIR spectra of nanocrystalline cellulose with absorption peaks at 3451 cm^{-1} and 2899 cm^{-1} which were ascribed to O-H and C-H stretching

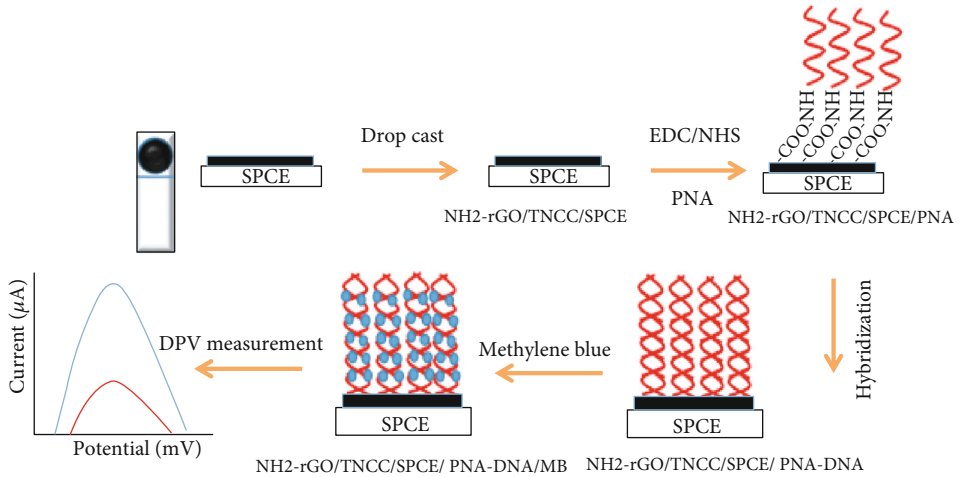

Schematic 1: The stepwise experimental procedure for fabrication of the PNA electrochemical biosensor.

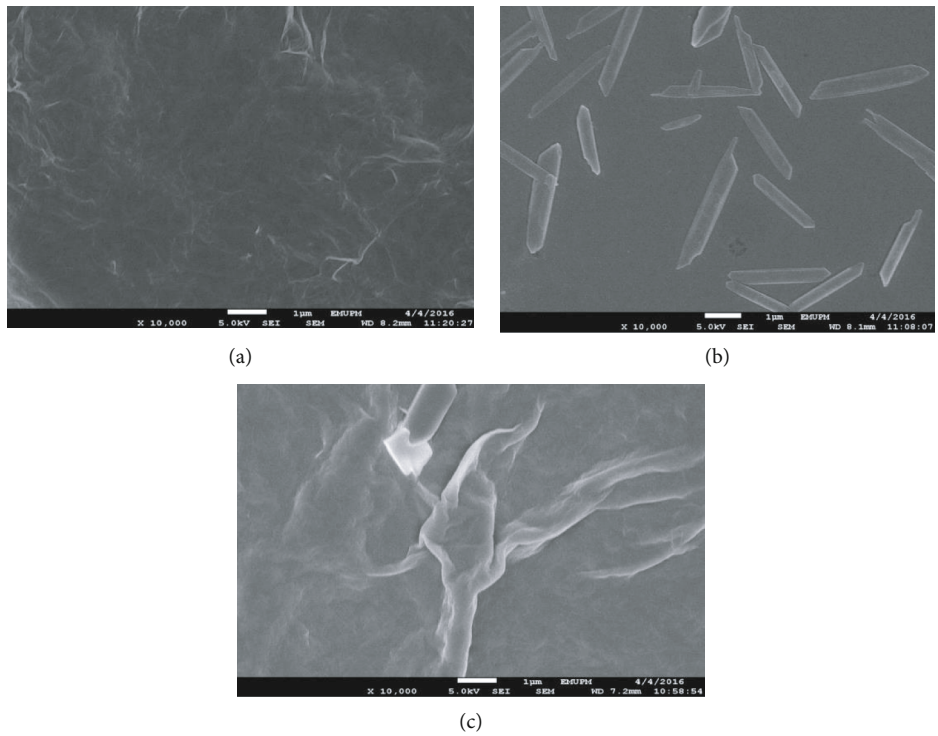

(a) (b) (c)

Figure 1: FESEM images of (a) NH_2-rGO, (b) TNCC, and (c) NH_2-rGO/TNCC.

vibrations, respectively. Subsequently, other peaks in the range of 1410–1420 cm^{-1} is resulted from CH_2 scissoring motion in cellulose [40], while the absorption peak at 1060 cm^{-1} indicates the vibration of C-O-C in the pyranose ring [41, 42]. Figure 2(b) shows that the FTIR spectrum of TEMPO-nanocrystalline nanocellulose (TNCC) displays a prominent peak at 1630 cm^{-1} representing carbonyl (C=O) stretching peak due to –COOH groups formed during TEMPO-mediated oxidation reaction [43].

While in Figure 2(c), FTIR spectra for NH_2-rGO show a new medium peak at 875 cm^{-1} representing N-H wag (1° amine) due to amidation reaction after GO treated with an amine. Moreover, double peaks also appeared at 2890 cm^{-1} and 3354 cm^{-1}, corresponding to the $-CH_2$ stretching vibration and N-H stretch of primary amine groups that originated from the ethylenediamine [38, 44]. Furthermore, Figure 2(d) shows the FTIR spectra of NH_2-rGO/TNCC with a small peak observed at 1690 cm^{-1} which is assigned to the C=O stretching vibration of –NHCO– (amide I) [45]. It can be seen that the peaks at 1630 cm^{-1} was less visible compared to FTIR spectra in Figure 2(b) due to consumption of –COOH groups during amidation reaction between NH_2-GO and TNCC. A small peak at 1251 cm^{-1} corresponds to C–O stretching vibration of the carboxyl group which suggested the excessive COOH-group due to TEMPO-oxidation reaction [46, 47].

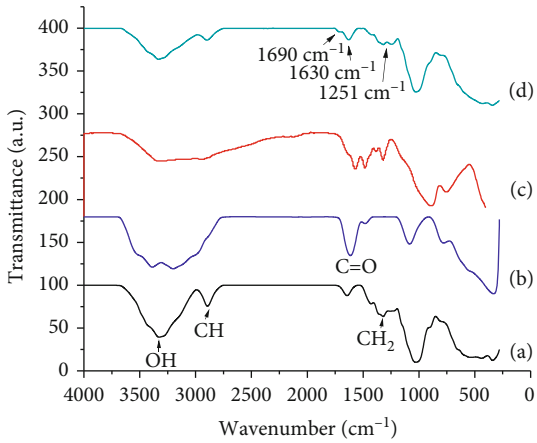

FIGURE 2: FTIR spectra of (a) nanocrystalline cellulose, (b) TEMPO-nanocrystalline nanocellulose (TNCC), (c) NH_2-rGO, and (d) NH_2-rGO/TNCC.

3.3. Electrochemical Characterization of the Modified Electrode. Various modified electrodes were monitored in 5 mM ferro-/ferricyanide ($Fe(CN)_6^{4-/3-}$) containing 0.1 M KCl by cyclic voltammetric as shown in Figure 3(a). In this study, bare SPE shows a distinct redox peak of $Fe(CN)_6^{-4/-3}$ (curve (A), orange line) indicates a reversible and well-defined system. After the modification of the SPE with TNCC, no significant enhancement of current was recorded (curve (B), red line) likely due to a lack of conductivity properties. However, slight decrease in peak-to-peak separation (ΔEp) was observed indicating that the modification of the SPCE with nanohybrid material has improved reversibility of the electron transfer process (curve (C), blue line) [48]. Interestingly, modification of SPE with NH_2-rGO/TNCC shows a significant increase of peak current with the peak-to-peak separation (ΔEp) about 274 mV. This phenomenon indicates the excellent conductivity properties of NH_2-rGO/TNCC due to the accomplishment of diffusional control by $Fe(CN)_6^{3-/4-}$ ion on the surface of the electrode [49]. These results were further confirmed by the EIS measurements according to equivalent circuit Randle's model, which was found to accurately fit the experimental data as shown in Figure 3(b). The components in the equivalent circuit consist of solution resistance (Rs), charge-transfer resistance (Rct), constant phase element (CPE), and Warburg impedance (Zw) as can be seen in the inset of Figure 3(b). It can be noted that the Nyquist plot of bare SPE electrode shows large semicircle domain (curve (A)) with Rct about 18.2 kΩ. Meanwhile, TNCC/SPE (curve (B)) shows that the Rct value was decreased to about 10.9 kΩ suggested that a high surface area of TNCC/SPE enables for shuttling electron between the electrode and ferri/ferrocyanide ($[Fe(CN)_6]^{3-/4-}$) ions. The presence of polar water groups and the free charges accumulated at the interfaces of NCC has facilitated the flow of current and enhances electrical conductivity [50]. Furthermore, NH_2-rGO/TNCC/SPE shows a small well-defined semicircle (curve (C)) which implies the lowest electron-transfer resistance (4.5 kΩ). The obtained result was suggesting that NH_2-rGO was the main contributor to lower the resistance value of the electrode due to the higher electrical conductivity properties of NH_2-rGO. Subsequently, the electroactive surface area of the electrode was determine by exploring the oxidation peak current with a scan rate as shown in Figure 3(c). Subsequently, Randles-Sevcik equation (1) [51] was applied as follows:

$$\mathrm{Ipa} = \frac{\left(2.69 \times 10^5\right) n^3}{{}^2\mathrm{V}^{1/2}\mathrm{D}^{1/2}\mathrm{AC}}, \quad (1)$$

where Ipa is the oxidation peak current (A), n is the electron transfer number of $K_3[Fe(CN)_6]$, A is the electroactive surface electrode area (cm^2), D is the diffusion coefficient of $K_3[Fe(CN)_6]$ (cm^2 s^{-1}), C is the concentration for $K_3[Fe(CN)_6]$, and V is the scan rate. According to this calculation, the average electroactive surface area of the bare SPE and NH_2-rGO/TNCC/SPE were calculated to be 0.08 cm^2 and 0.163 cm^2, respectively, indicating that the electroactive surface area of the electrode was increased after the modification step.

3.4. Electrochemical Behavior of MB on the Modified Electrodes. The catalytic activity of NH_2-rGO/TNCC/SPE towards methylene blue (MB) was investigated by the cyclic voltammetric in three different conditions: (a) without ssPNA, (b) in the presence of ssPNA (5 μM), and (c) in the presence of PNA together with the MTB DNA target concentration introduced (1×10^{-8} M), respectively. As shown in Figure 4(a), anodic peak potential at −0.26 V (curve (A), black line) has shown a reversible electron transfer reaction even without ssPNA on surface of the modified electrode, which can be attributed to the electrochemical reaction of the phenothiazine group [52]. Interestingly, CV peak displayed the negatively shifted peak, and increases of peak current after ssPNA were immobilized on the modified electrode (curve (B), blue line), which indicated that MB can be transported through ssPNA. The dependence of methylene blue and DNA has been studied with various methods with at least three different interaction mechanisms reported. These include electrostatic interaction between cationic MB and anionic DNA, intercalation of MB in the DNA double helix, and preferential binding between MB and guanine bases [53, 54]. However, in this study, electrostatic interaction appears to be a weaker interaction due to the neutral charge of PNA. Therefore, intercalation and preferential binding might play a notable role for MB to interact with DNA-PNA in this study. Furthermore, the achievement of hybridization reaction on the surface of the modified electrode leads to huge increased of oxidation peak current (curve (C), red line). This result is contradicting with other researches, which shown that hybridization leads to a decrement of current. The different results produced in previous studies could be due to the orientation conformation of the oligomer PNA probe after being immobilized on the surface of the electrode. Considering the fact that standing up oligomer PNA probe orientation likely would lead to the increment of the current signal where MB easily can interact with the guanines in DNA duplex formation, lying down oligomer probe orientation would lead to the decrement of

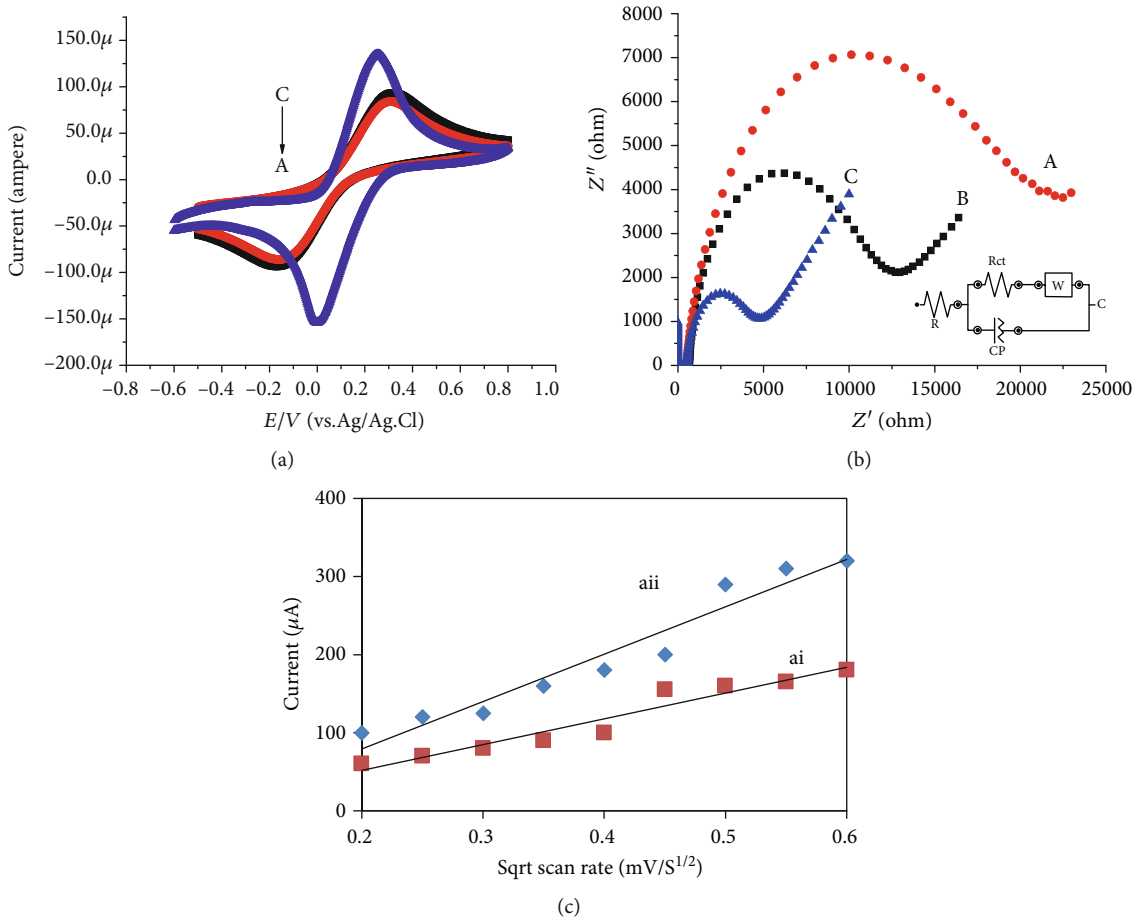

Figure 3: Cyclic voltammograms (a). Electrochemical impedance spectroscopy (EIS) (b) of (A) bare SPE, (B) TNCC/SPE, and (C) NH_2-rGO/TNCC/SPE in the probing electrolyte of 5.0 mM $K_4Fe(CN)_6/K_3Fe(CN)_6$ with 0.1 M KCl at a scan rate of 100 mV s^{-1}. (c) The plot of oxidation peak current of $(Fe(CN)_6)^{3-/4-}$ of (ai) bare SPE and (aii) NH_2-rGO/TNCC/SPE against square roots of a scan rate.

current as the interaction between MB and guanine is inhibited by the wrapped guanine [55, 56].

Furthermore, the effect of MB concentration and immersion time was also studied on NH_2-rGO/TNCC/SPE/PNA with concentration of ssDNA target was fixed at 1 μM. In Figure 4(b), the concentration of MB was studied ranging from 15 μM to 55 μM and maximum concentration of MB was obtained at 45 μM. Above MB concentration of 45 μM, slightly decreased on NH_2-rGO/TNCC/SPE/PNA-DNA response was observed which indicated saturation point of MB molecules accumulated into double-stranded DNA. While in Figure 4(c), effect of MB immersion time shows the DPV current response increased as the immersion time was increased. However, the DPV current response displays decay of current at immersion time more than 5 min. This observation was attributed to interaction between guanine bases, and MB has achieved saturation point, thereby hindered the diffusion of MB molecule to the electrode surface due to excessive MB molecule and resulted in the decrease of peak current. Thus, the optimum concentration of MB and immersion time of MB of 45 μM and duration of 5 min were selected for further study.

3.5. Selectivity and Sensitivity of the PNA Biosensor. The selectivity of the fabricated biosensor was investigated using different types of ssDNA target sequence related to *M. tuberculosis* which consists of complementary, noncomplementary, and 1-base mismatch sequence, respectively. The concentration of all targets sequence was fixed at 1×10^{-8} M. Figure 5(a) shows that the DPV peak current with a relatively small response was observed after hybridized with noncomplimentary DNA (curve (B)) which may attribute to the nonspecific hybridization between ssPNA and target DNA on the surface of bioelectrode [57]. Meanwhile, the discrimination against hybridization with one-base mismatch DNA approximately 30% of that noncomplementary indicated incomplete hybridization between the probe and single-base mismatch. As a result, the highest current response of MB was obtained when ssPNA exposed to complementary DNA target sequence which indicated the formation of hybridized PNA-DNA on the surface of the modified electrode. This result demonstrated the ability of the proposed biosensor to distinguish complementary, noncomplementary, and one-base mismatch sequences, respectively.

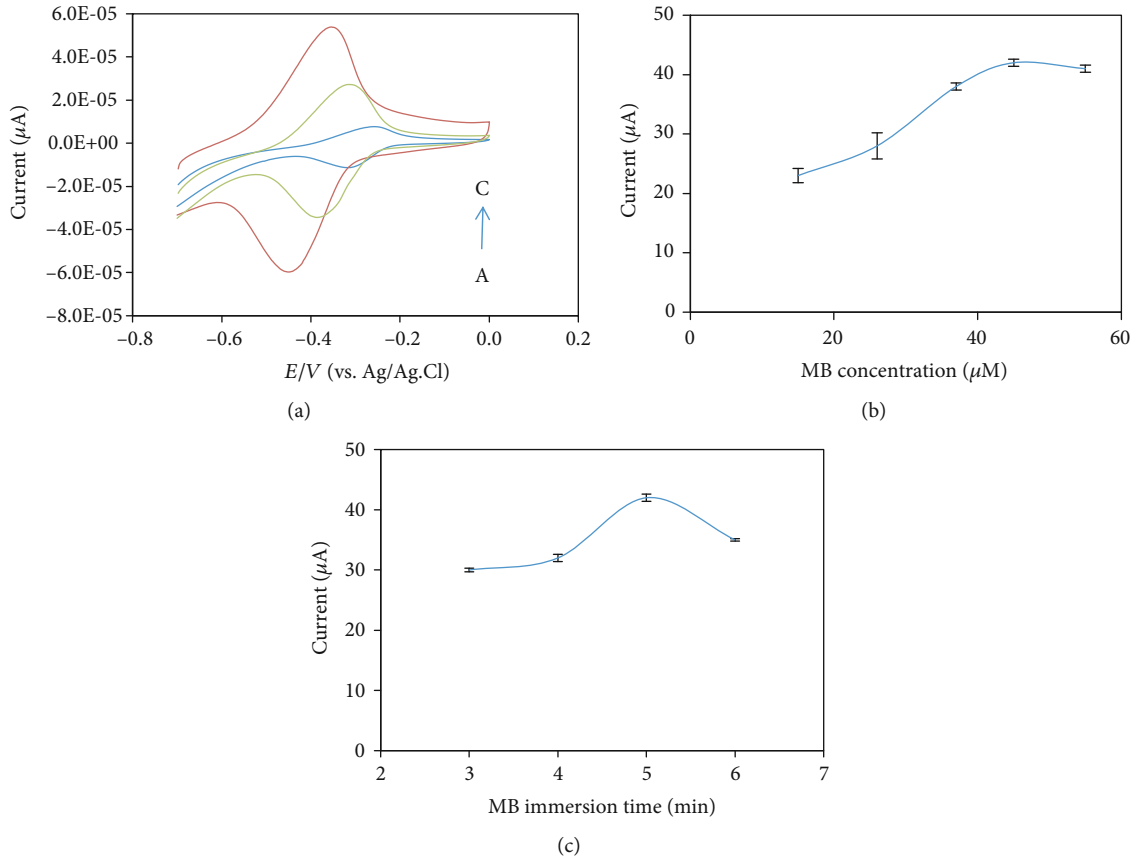

FIGURE 4: (a) Cyclic voltammetry of methylene blue (MB) on NH_2-rGO/TNCC/SPCE: (A) without a PNA probe, (B) with a PNA probe, and (C) with PNA together with the MTB DNA target concentration introduced was 1×10^{-8} M. (b) Optimization of methylene blue (MB) concentrations. (c) Optimization of immersion time.

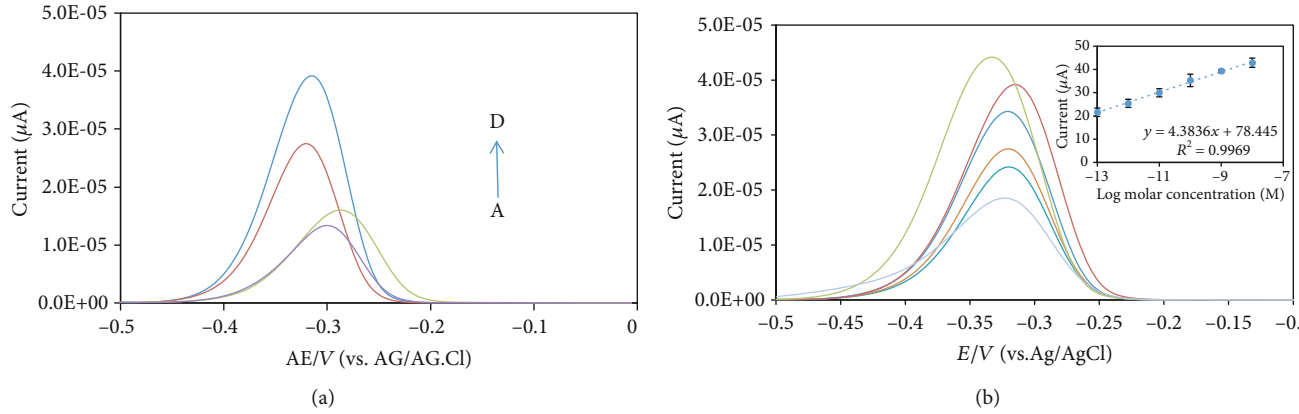

FIGURE 5: (a) Selectivity of the PNA biosensor investigated with different types of DNA: (A) PNA only, (B) noncomplimentary, (C) one-base mismatch, and (D) complimentary; DPV curve at different concentrations of complementary DNA; (b) linear relationship between DPV peak current (I_p) with the different concentrations of complementary DNA of 1×10^{-13} M – 1×10^{-8} M (from (F) to (A)) in 0.1 M phosphate buffer solution (inset: enlarge view of the calibration plot in the concentration range of 1×10^{-13} M – 1×10^{-8} M of DNA target).

Under the optimum condition, the electrochemical PNA biosensor was hybridized with different concentrations of ssDNA target sequences related to *M. tuberculosis* and the changes pattern in current signal was observed. From the result, the peak current of MB increases gradually with the increase of ssDNA target concentration in the range of 1×10^{-13} M–1×10^{-8} M with the regression equation of $y = 4.3836x + 78.445$ (Figure 5(b) (inset)); where y is peak current (μA), x is ssDNA target concentration; the detection limit of the fabricated sensor was calculated to be at 3.14×10^{-14} M using $3\sigma/m$ measurement (σ: standard deviation of blank solution; m: slope) [58]. As illustrated

Table 1: Comparison of the present work and other reported techniques for the determination of *M. tuberculosis*.

Electrode	Probe	Nanocomposite	Limit of detection (LOD)	Redox indicator	Reference
GCE	PNA	RGO	1.0×10^{-13} M	MB	[57]
ITO	DNA	Au/RGONR	0.10×10^{-15} M	$[Fe(CN)_6]^{3-/4-}$	[58]
GCE	DNA	Graphene-gold polyaniline	5.45×10^{-13} M	$Fe(CN)_6^{4-/3-}$	[60]
SPE	DNA	RGO/quantum dots	8.95×10^{-13} M	MB	[36]
SPE	DNA	Polyaniline/graphene	7.85×10^{-7} M	MB	[59]
SPE	PNA	NH_2-rGO/TEMPO-nanocellulose	3.14×10^{-14} M	MB	This work

Note: GCE: glassy carbon electrode; SPE: screen-printed electrode; ITO: indium tin oxide; RGO: reduced graphene oxide; Au/RGO NR: gold nanoparticles/reduced graphene oxide nanoribbons; $Fe(CN)_6^{4-/3-}$: ferro-/ferricyanide; MB: methylene blue.

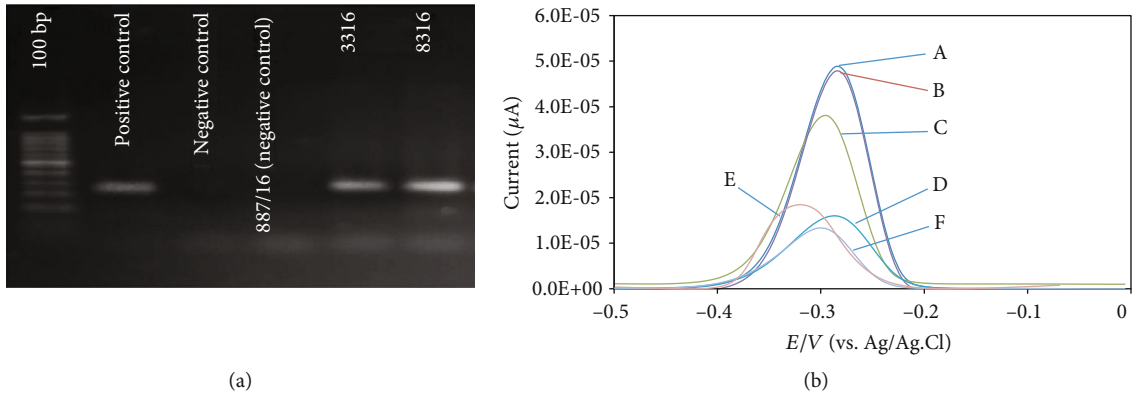

(a) (b)

Figure 6: (a) PCR gel electrophoresis. (b) DPV curves for the detection for (A) (3316), (B) (8316), (C) (positive control), (D) (negative control), (E) (negative sample), and (F) (blank).

in Table 1, a comparison with other reported electrochemical biosensors for the detection of *Mycobacterium tuberculosis*, the limit of detection obtained by the developed biosensor was slightly better and comparable with other biosensors [36, 57–60].

In addition, the reproducibility study of the biosensor has been investigated using complementary DNA target concentration of 1.0×10^{-8} M (data not shown). Five replicates of NH_2-rGO/TNCC/ssPNA/SPCE were used for the evaluation, and the relative standard deviation (RSD) of 4.46% ($n = 5$) was obtained indicating a satisfactory reproducibility of the fabricated PNA biosensor. For storage stability study, the biosensor was stored at 4°C and its relative response was measured periodically for 35 days. The sensor response was recorded as a function of time, and it remained stable for about 80% of its initial response after 35 days of storage.

3.6. Detection with the PCR Product of M. tuberculosis. Figure 6(a) exhibits that the gel electrophoresis of *M. tuberculosis* images of the PCR analysis had successfully performed and the fragment was about 245 bp after the amplification. The obtained product was diluted with phosphate buffer solution (pH 7) and denatured by heating in a boiling water for 10 min in water bath. Then, 2 μL of the denatured PCR amplification product was dropped directly onto the PNA biosensor for the hybridization process. After hybridization, the electrode was immersed into MB solution for the detection. Figure 6(b) shows DPV response of the PNA electrochemical biosensor after being hybridized with PCR-amplified sample of *M. tuberculosis* with different kinds of DNA for 50 min, which consists of positive control, negative control, negative sample, positive MTB 1 (8316), and positive MTB 2 (3316). The DPV result also shows that highest electrochemical current responses were obtained after hybridization with positive MTB 1 (curve (A)), followed by positive MTB 2 (curve (B)), and positive control sample, respectively, due to the specific DNA binding. As expected, obvious decreases of MB oxidation current after hybridization with negative control (curve (E)) and negative sample occurred (curve (F)) is due to nonspecific hybridization. The outcome of this work shows that the constructed PNA biosensor exhibited good selectivity towards different types of DNA related to MTB and the modified electrode. As shown the fabricated sensor could be further applied for the effective detection of *M. tuberculosis* sequences in PCR-amplified samples.

4. Conclusion

An electrochemical PNA biosensor was successfully developed based on nanohybrid material of amine functionalized reduced graphene oxide (NH_2-rGO) and TEMPO-nanocrystalline cellulose (TNCC) for the detection of *M.*

Tuberculosis. In this research, the utilization of PNA as a probe for the detection of the complementary target of *M. tuberculosis* using DPV was linear in the concentration range of 1×10^{-8} M to 1×10^{-13} M with the detection limit of 3.14×10^{-14} M. The results showed good electrochemical activity with high sensitivity and specificity with synthetic DNA, which was then extended to analyze real-world PCR products. The proposed PNA electrochemical biosensor has shown promising features for the detection of *M. tuberculosis* which can be applied to the direct detection of the PCR product from the sputum sample.

Data Availability

The data used to support the findings of this study are included within the article.

Conflicts of Interest

The authors declare that there is no conflict of interests.

Acknowledgments

The authors are grateful for the financial support provided by the Ministry of Education Malaysia through Universiti Putra Malaysia under Geran Putra IPB (GP-IPB/2013/9412700) and Ministry of Science, Technology and Innovation under Science Fund (03-01-04-SF2045).

References

[1] A. Sakula, "Robert Koch: centenary of the discovery of the tubercle bacillus, 1882," *Thorax*, vol. 37, no. 4, pp. 246–251, 1982.

[2] World Health Organization, "Global Tuberculosis Report, 214," 2017, http://www.who.int/tb/publications/global_report/en/.

[3] M. Raviglione and G. Sulis, "Tuberculosis: burden, challenges and strategy for control and elimination infect," *Infectious Disease Reports*, vol. 8, no. 2, p. 6570, 2016.

[4] R. E. Huebner, M. F. Schein, and J. B. Bass Jr., "The tuberculin skin test," *Clinical Infectious Diseases*, vol. 17, no. 6, pp. 968–975, 1993.

[5] G. Aderaye, H. G/Egziabher, A. Aseffa, A. Worku, and L. Lindquist, "Comparison of acid-fast stain and culture for *Mycobacterium tuberculosis* in pre- and post-bronchoscopy sputum and bronchoalveolar lavage in HIV-infected patients with atypical chest X-ray in Ethiopia," *Annals of Thoracic Medicine*, vol. 2, no. 4, pp. 154–157, 2007.

[6] G. Kaguthi, V. Nduba, J. Nyokabi, F. Onchiri, R. Gie, and M. Borgdorff, "Chest radiographs for pediatric TB diagnosis: interrater agreement and utility," *Interdisciplinary Perspectives on Infectious Diseases*, vol. 2014, Article ID 291841, 8 pages, 2014.

[7] D. Parashar, D. S. Chauhan, V. D. Sharma, and V. M. Katoch, "Applications of real-time PCR technology to mycobacterial research," *Indian Journal of Medical Research*, vol. 124, no. 4, pp. 385–398, 2006.

[8] R. Kaur, K. Kachroo, J. K. Sharma, S. M. Vatturi, and A. Dang, "Diagnostic accuracy of Xpert test in tuberculosis detection: a systematic review and meta-analysis," *Journal of Global Infectious Diseases*, vol. 8, no. 1, pp. 32–40, 2016.

[9] L. Zhou, X. He, D. He, K. Wang, and D. Qin, "Biosensing Technologies for *Mycobacterium tuberculosis* Detection: Status and New Developments," *Clinical and Developmental Immunology*, vol. 2011, Article ID 193963, 8 pages, 2011.

[10] S.-H. Hsu, Y.-Y. Lin, S.-H. Lu, I.-F. Tsai, Y.-T. Lu, and H.-T. Ho, "*Mycobacterium tuberculosis* DNA detection using surface plasmon resonance modulated by telecommunication wavelength," *Baseline*, vol. 14, no. 1, pp. 458–467, 2014.

[11] M. Jaramillo, Y. J. Montagut, A. Montoya et al., "Design of a piezoelectric immunosensor for tuberculosis biomarker detection," in *Conference Pan American Health Care Exchanges (PAHCE)*, Medellin, Colombia, 29 April-4 May 2013.

[12] H. Mukundan, S. Kumar, D. N. Price et al., "Rapid detection of *Mycobacterium tuberculosis* biomarkers in a sandwich immunoassay format using a waveguide-based optical biosensor," *Tuberculosis*, vol. 92, no. 5, pp. 407–416, 2012.

[13] R. Guntupalli, J. Hu, R. S. Lakshmanan, T. S. Huang, J. M. Barbaree, and B. A. Chin, "A magnetoelastic resonance biosensor immobilized with polyclonal antibody for the detection of *Salmonella typhimurium*," *Biosensors and Bioelectronics*, vol. 22, no. 7, pp. 1474–1479, 2007.

[14] R. Mcnerney and P. Daley, "Towards a point-of-care test for active tuberculosis: obstacles and opportunities," *Nature Reviews Microbiology*, vol. 9, no. 3, pp. 204–213, 2011.

[15] N. A. Hamdan, R. Issa, M. F. M. Noh, and N. M. Zin, "Electrochemical technique using methylene blue with pencil graphite electrode for optimum detection of *Mycobacterium tuberculosis* DNA," *Current Research in Tuberculosis*, vol. 4, no. 1, pp. 1–12, 2012.

[16] J. Wang, "DNA biosensors based on Peptide Nucleic Acid (PNA) recognition layers. A review[1]," *Biosensors and Bioelectronics*, vol. 13, no. 7-8, pp. 757–762, 1998.

[17] K. E. Mach, A. M. Kaushik, K. Hsieh, P. K. Wong, T. H. Wang, and J. C. Liao, "Optimizing peptide nucleic acid probes for hybridization-based detection and identification of bacterial pathogens," *The Analyst*, vol. 144, no. 5, pp. 1565–1574, 2019.

[18] P. E. Nielsen and M. Egholm, "An introduction to peptide nucleic acid," *Current Issues in Molecular Biology*, vol. 1, no. 2, pp. 89–104, 1998.

[19] F. Pellestor and P. Paulasova, "The peptide nucleic acids (PNAs), powerful tools for molecular genetics and cytogenetics," *European Journal of Human Genetics*, vol. 12, no. 9, pp. 694–700, 2004.

[20] F. T. C. Moreira, M. J. M. S. Ferreira, J. R. T. Puga, and M. G. F. Sales, "Screen-printed electrode produced by printed-circuit board technology. Application to cancer biomarker detection by means of plastic antibody as sensing material," *Sensors and Actuators B: Chemical*, vol. 223, pp. 927–935, 2016.

[21] O. D. Renedo, M. A. Alonso-Lomillo, and M. J. A. Martínez, "Recent developments in the field of screen-printed electrodes and their related applications," *Talanta*, vol. 73, no. 2, pp. 202–219, 2007.

[22] S. Zhang, G. Wright, and Y. Yang, "Materials and techniques for electrochemical biosensor design and construction," *Biosensors and Bioelectronics*, vol. 15, no. 5-6, pp. 273–282, 2000.

[23] M. D. Sonawane and S. B. Nimse, "Surface modification chemistries of materials used in diagnostic platforms with

biomolecules," *Journal of Chemistry*, vol. 2016, Article ID 9241378, 19 pages, 2016.

[24] S. F. D'Souza, "Immobilization and stabilization of biomaterials for biosensor applications," *Biotechnology and Applied Biochemistry*, vol. 96, no. 1-3, pp. 225–238, 2001.

[25] M. D. Tezerjani, A. Benvidi, M. Rezaeinasab et al., "An impedimeric biosensor based on a composite of graphene nanosheets and polyaniline as a suitable platform for prostate cancer sensing," *Analytical Methods*, vol. 8, no. 41, pp. 7507–7515, 2016.

[26] J. George and S. N. Sabapathi, "Cellulose nanocrystals: synthesis, functional properties, and applications," *Nanotechnology, Science and Applications*, vol. 8, pp. 45–54, 2015.

[27] N. Lin and A. Dufresne, "Nanocellulose in biomedicine: current status and future prospect," *European Polymer Journal*, vol. 59, pp. 302–325, 2014.

[28] C. Esmaeili, M. Abdi, A. Mathew, M. Jonoobi, K. Oksman, and M. Rezayi, "Synergy effect of nanocrystalline cellulose for the biosensing detection of glucose," *Sensors*, vol. 15, no. 10, pp. 24681–24697, 2015.

[29] J. Peña-Bahamonde, H. N. Nguyen, S. K. Fanourakis, and D. F. Rodrigues, "Recent advances in graphene-based biosensor technology with applications in life sciences," *Journal of Nanobiotechnology*, vol. 16, no. 1, p. 75, 2018.

[30] R. Malviya, P. K. Sharma, and S. K. Dubey, "Modification of polysaccharides: pharmaceutical and tissue engineering applications with commercial utility (patents)," *Materials Science and Engineering: C*, vol. 68, pp. 929–938, 2016.

[31] D. Chen, H. Feng, and J. Li, "Graphene oxide: preparation, functionalization, and electrochemical applications," *Chemical Reviews*, vol. 112, no. 11, pp. 6027–6053, 2012.

[32] P. T. Yin, S. Shah, M. Chhowalla, and K. B. Lee, "Design, Synthesis, and Characterization of Graphene–Nanoparticle Hybrid Materials for Bioapplications," *Chemical Reviews*, vol. 115, no. 7, pp. 2483–2531, 2015.

[33] A. Benvidi, N. M. Saucedo, P. Ramnani et al., "Electro-oxidized monolayer CVD graphene film transducer for ultrasensitive impedimetric DNA biosensor," *Electroanalysis*, vol. 30, no. 8, pp. 1791–1800, 2018.

[34] R. Issa, N. A. Hamdan, and M. F. M. Noh, "Differential pulse voltammetric determination of DNA hybridization using methylene blue on screen printed carbon electrode for the detection of *Mycobacterium tuberculosis*," *Biotechnology Journal*, vol. 9, no. 3, pp. 304–311, 2010.

[35] H. Fukuzumi, T. Saito, S. Iwamoto et al., "Pore size determination of TEMPO-oxidized cellulose nanofibril films by positron annihilation lifetime spectroscopy," *Biomacromolecules*, vol. 12, no. 11, pp. 4057–4062, 2011.

[36] M. H. Mat Zaid, J. Abdullah, N. A. Yusof et al., "PNA biosensor based on reduced graphene oxide/water soluble quantum dots for the detection of *Mycobacterium tuberculosis*," *Sensors and Actuators B: Chemical*, vol. 241, pp. 1024–1034, 2017.

[37] N. H. Kim, T. Kuila, and J. H. Lee, "Simultaneous reduction, functionalization and stitching of graphene oxide with ethylenediamine for composites application," *Journal of Materials Chemistry A*, vol. 1, no. 4, pp. 1349–1358, 2013.

[38] H. L. Ma, Y. Zhang, Q. H. Hu, D. Yan, Z. Z. Yu, and M. Zhai, "Chemical reduction and removal of Cr(vi) from acidic aqueous solution by ethylenediamine-reduced graphene oxide," *Journal of Materials Chemistry*, vol. 22, no. 13, p. 5914, 2012.

[39] T. Saito, S. Kimura, Y. Nishiyama, and A. Isogai, "Cellulose nanofibers prepared by TEMPO-mediated oxidation of native cellulose," *Biomacromolecules*, vol. 8, no. 8, pp. 2485–2491, 2007.

[40] M. Salajkova, L. A. Berglund, and Q. Zhou, "Hydrophobic cellulose nanocrystals modified with quaternary ammonium salts," *Journal of Materials Chemistry*, vol. 22, no. 37, pp. 19798–19805, 2012.

[41] A. Mandal and D. Chakrabarty, "Isolation of nanocellulose from waste sugarcane bagasse (SCB) and its characterization," *Carbohydrate Polymers*, vol. 86, no. 3, pp. 1291–1299, 2011.

[42] B. Soni, E. B. Hassan, and B. Mahmoud, "Chemical isolation and characterization of different cellulose nanofibers from cotton stalks," *Carbohydrate Polymers*, vol. 134, no. 10, pp. 581–589, 2015.

[43] D. da Silva Perez, S. Montanari, and M. R. Vignon, "TEMPO-mediated oxidation of cellulose III," *Biomacromolecules*, vol. 4, no. 5, pp. 1417–1425, 2003.

[44] X. Hu, J. Xu, C. Wu et al., "Ethylenediamine grafted to graphene oxide@Fe_3O_4 for chromium (VI) decontamination: Performance, modelling, and fractional factorial design," *Plos One*, vol. 12, no. 10, pp. 1–14, 2017.

[45] R. D. S. Bezerra, R. C. Leal, M. S. da Silva et al., "Direct Modification of Microcrystalline Cellulose with Ethylenediamine for Use as Adsorbent for Removal Amitriptyline Drug from Environment," *Molecules*, vol. 22, no. 11, p. 2039, 2039.

[46] C. Xu, J. Li, X. Wang et al., "Synthesis of hemin functionalized graphene and its application as a counter electrode in dye-sensitized solar cells," *Materials Chemistry and Physics*, vol. 132, no. 2-3, pp. 858–864, 2012.

[47] U. P. Agarwal, R. S. Reiner, and S. A. Ralph, "Cellulose I crystallinity determination using FT-Raman spectroscopy: univariate and multivariate methods," *Cellulose*, vol. 17, no. 4, pp. 721–733, 2010.

[48] W. Yantasee, G. E. Fryxell, and Y. Lin, "Voltammetric analysis of europium at screen-printed electrodes modified with salicylamide self-assembled on mesoporous silica," *Analyst*, vol. 131, no. 12, pp. 1342–1346, 2006.

[49] R. S. Nicholson, "Theory and application of cyclic voltammetry for measurement of electrode reaction kinetics," *Analytical Chemistry*, vol. 37, no. 11, pp. 1351–1355, 1965.

[50] J. Bard and L. R. Faulkner, *Electrochemical Methods and Its Application*, John Wiley and Sons, Inc., 2nd Ed edition, 2001.

[51] A. Ladhar, M. Arous, H. Kaddami et al., "Ionic hopping conductivity in potential batteries separator based on natural rubber-nanocellulose green nanocomposites," *Journal of Molecular Liquids*, vol. 211, pp. 792–802, 2015.

[52] P. O. Vardevanyan, A. P. Antonyan, M. A. Parsadanyan, M. A. Shahinyan, and L. A. Hambardzumyan, "Mechanisms for binding between methylene blue and DNA," *Journal of Applied Spectroscopy*, vol. 80, no. 4, pp. 595–599, 2013.

[53] S. O. Kelley, J. K. Barton, N. M. Jackson, and M. G. Hill, "Electrochemistry of methylene blue bound to a DNA-modified electrode," *Bioconjugate Chemistry*, vol. 8, no. 1, pp. 31–37, 1997.

[54] A. Erdem, K. Kerman, B. Meric, U. S. Akarca, and M. Ozsoz, "Novel hybridization indicator methylene blue for the electrochemical detection of short DNA sequences related to the hepatitis B virus," *Analytica Chimica Acta*, vol. 422, no. 2, pp. 139–149, 2000.

[55] J. I. A. Rashid, N. A. Yusof, J. Abdullah, U. Hashim, and R. Hajian, "The utilization of SiNWs/AuNPs-modified indium tin oxide (ITO) in fabrication of electrochemical DNA sensor," *Materials Science and Engineering C*, vol. 45, pp. 270–276, 2014.

[56] D. Pan, X. Zuo, Y. Wan et al., "Electrochemical interrogation of interactions between surface-confined DNA and methylene blue," *Sensors*, vol. 7, no. 11, pp. 2671–2680, 2007.

[57] D. Du, S. Guo, L. Tang, Y. Ning, Q. Yao, and G.-J. Zhang, "Graphene-modified electrode for DNA detection via PNA-DNA hybridization," *Sensors and Actuators B: Chemical*, vol. 186, pp. 563–570, 2013.

[58] N. K. Mogha, V. Sahu, R. K. Sharma, and D. T. Masram, "Reduced graphene oxide nanoribbon immobilized gold nanoparticle based electrochemical DNA biosensor for the detection of *Mycobacterium tuberculosis*," *Journal of Materials Chemistry B*, vol. 6, no. 31, pp. 5181–5187, 2018.

[59] F. Mohamad, M. M. Zaid, J. Abdullah et al., "Synthesis and characterization of polyaniline/graphene composite nanofiber and its application as an electrochemical DNA biosensor for the detection of *Mycobacterium tuberculosis*," *Sensors*, vol. 17, no. 12, p. 2789, 2017.

[60] C. Liu, D. Jiang, G. Xiang, L. Liu, F. Liu, and X. Pu, "An electrochemical DNA biosensor for the detection of *Mycobacterium tuberculosis*, based on signal amplification of graphene and a gold nanoparticle-polyaniline nanocomposite," *Analyst*, vol. 139, no. 21, pp. 5460–5465, 2014.